The Application of Fuzzy Logic Control to Balance a Wheelchair

Phichitphon Chotikunnan * **Benjamas Panomruttanarug** **

* *Department of Control Systems and Instrumentation Engineering, King Mongkuts University of Technology Thonburi, Bangkok Thailand. Tel.: +66-2-470-9096 (e-mail: phichitphon.cho@mail.kmutt.ac.th)*
** *Department of Control Systems and Instrumentation Engineering, King Mongkuts University of Technology Thonburi, Bangkok Thailand. Tel.: +66-2-470-9096 (e-mail: benjamas.pan@kmutt.ac.th)*

Abstract: The objective of this research project is to construct an affordable and durable stand-up wheelchair, which will enable wheelchair users to adjust the vertical height of their chair while still remaining seated. The mechanical design, together with the lifting mechanism, demonstrates the ability of the wheelchair to lift up the front wheels (casters), and ride solely on the rear wheels. The control structures of the wheelchairs, based on Fuzzy Logic Type-1 and Type-2, are aimed at enabling the user to maintain stability when moving on two wheels. This project will compare simulation and experimental results to illustrate the effectiveness of each control scheme. An experimental study of riding on different levels of roughness is also provided.

Keywords: wheelchair, balancing, fuzzy logic, interval type-2, TSK

1. INTRODUCTION

The iBOT is an electric powered wheelchair that was developed by Dean Kamen and other engineers at DEKA research & development corporation in the 1990s (iBOT). It is not only designed to provide mobility for disabled users, but it has also been designed to provide several unique advantages over a traditional electric wheelchair. One of the significant advantages is that it will enable disabled people who use the iBOT wheelchair, to lift themselves up so they can reach certain heights in confined spaces, for example, to put things on shelves, or to have conversations with other people at eye-to-eye level.

In order to raise the chair up so it can reach higher levels, the wheelchair has to be on two-wheels. This can be achieved by lifting up the front wheels (casters) of the wheelchair so that the wheelchair is elevated into an upright position. When the wheelchair is on two wheels, it performs as a double inverted pendulum, and therefore, it is characterized as being a highly non-linear complex unstable system. For this reason, suitable controls are required in order to lift and stabilize the two-wheeled wheelchair in the upright position.

There is not an abundance of research literature describing how to model and control a two-wheeled wheelchair. (Ahmad et al., 2014) developed a non-linear model for a two-wheeled wheelchair, using state space representation. The proposed model was verified by using a simulation, which demonstrated the effectiveness of the estimation method. In addition, (Ahmad et al., 2011) provided a design, and also showed the implementation method of the fuzzy logic control, to lift and stabilize a wheelchair that is standing on two wheels into an upright position. The wheelchair was modeled and controlled while imitating a double inverted pendulum problem. For this experiment, only simulation results were provided to validate the design architecture. In (ZL et al., 2006), a comparison of the dynamic performance of the three self-balancing wheelchair (SBW) designs: (i) the hanging pendulum counterweight (HPC); (ii) the single inverted pendulum (SIP); and (iii) the double inverted pendulum (DIP), was conducted, with all three designs being controlled by a common state space controller. This comparison illustrated that the HPC design performed best, based on stability and performance factors.

A similar research topic, involving the control of a double inverted pendulum on a cart, has been studied in much greater detail. In (Yi et al., 2002; Yi et al., 2001b), it proposed a fuzzy controller that has the ability to stabilize a double inverted pendulum system, while also providing a wide range of initial angles for the two pendulums. In (Mon and Lin, 2014; Tao et al., 2010), a fuzzy logic based control was combined with a sliding control technique, to maintain the stability of the double inverted pendulum system. In contrast, other literature, such as, have not focused on stable equilibrium control, but rather, they have focused on how to perform a swing up maneuver in a double inverted pendulum system. In (Rubi et al., 2002), a gain scheduling linear optimal controller was used to track the desired trajectory, while performing a task that required it to swing up. Simulation and experimental results were used to demonstrate the effectiveness of the approach. In (Graichen et al., 2007), the performance of the same swing up maneuver, using a feedback control with linear methods, was also demonstrated in an experiment.

A simpler topic, which focused on a single inverted pendulum control, has received significant attention over the past decade. Segway represents a well-known self-balancing two-wheeled vehicle innovation, based on a single inverted pendulum control (Segway). A large number of publications have presented control strategies, which maintain the stability of a wheelchair in an upright position. The approach that was adopted, included state feedback control methods (Bettayeb et al., 2014; Bettayeb et al., 2001; Ibáñez et al., 2012), non-linear control methods (Aracil et al., 2013; Durand et al., 2013), sliding mode control methods (Adhikary and Mahanta, 2013), and also intelligent control methods, such as neural network (Noh et al., 2010) and fuzzy logic (Bardini and Nagar, 2014; Yi et al., 2001a). The different types of controllers that have been designed to achieve self-balancing for wheelchairs, have been investigated and summarized (Chan et al., 2013).

Our previous work (Panomruttanarug and Chotikunnan, 2014) develops a stabilizing control mechanism to maintain stability of a wheelchair in an upright position. The stabilizing control mechanism is based on a design of fuzzy logic control, since this method is capable of handling uncertainties that may arise in situations where it is difficult to decide on how to react. In respect to real application, precise knowledge of the dynamic system model is still lacking, and uncertainties arising from sensor noise have also been presented. Therefore, fuzzy logic control could handle any uncertainties arising from this problem. However, the previous paper only showed simulation results to present how effective the fuzzy control design performed, without considering uncertainties and input constraints. In this paper, by extending those results (Panomruttanarug and Chotikunnan, 2014), we focus directly on how to implement the design control to deal with a real life problem in the presence of input constraints and uncertainties. The main contributions of this paper are as follows: i) a prototype of a stand-up wheelchair including a mechanism that can lift up the front wheels has been developed; ii) for practical purposes, we modified the stabilizing control structure by introducing a Kalman filter to obtain accurate data from noisy sensors, and implemented the control structure to the wheelchair prototype using low-cost processors to achieve a stable upright position in real time. Noise covariance matrices in the Kalman filtering are adaptable based on the observation of wheelchair behaviors; iii) a comparative study using the practical control scheme is achieved by operating the wheelchair on different floor surfaces.

The remainder of this research paper is constructed as follows: Section 2 will describe the wheelchair mechanical design, lifting mechanism, and mathematical model in a state space representation. Section 3 will present fuzzy logic controllers that have been designed to stabilize a wheelchair on two wheels. In Section 4, an angular position estimation, using Kalman filtering, is stated. Simulation and experimental results have also been conducted to show the effectiveness of the control algorithm in Section 5. Finally, the conclusions of the findings will be presented in Section 6.

2. THE WHEELCHAIR

This section describes a design of a wheelchair and its mathematical model, when it is mobilized on two wheels.

2.1 Wheelchair structure

Figure 1 shows a wheelchair structure that has been created by using computer-aided design software (Catia). The wheelchair has three degrees of freedom, e.g., forward/backward, pitch, and yaws, driven by five DC motors. The first two motors are used to drive the left and right rear wheels in order to control motion (linear and steering). The next two motors are used to lift the front wheels (casters) to an upright position. In order to achieve the upright position, it requires certain amounts of torque to lift the front wheels. The last motor is connected to heavy loads, and it is designed to shift the center of gravity (COG) of the wheelchair back and forth when transitioning.

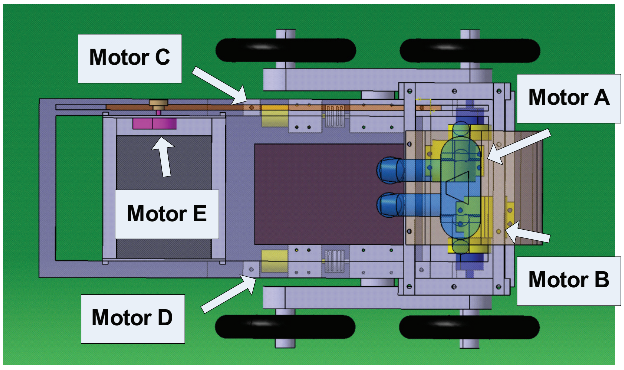

Fig. 1. Structure of wheelchair

2.2 From a sitting to standing position

In order to drive on two-wheels, the wheelchair is initially set to four-wheel function. The movable platform, containing packs of batteries and motors, is then slid backward, thus causing the COG to push toward to the rear wheels. When the COG is located over the rear wheels, the front wheels (casters) begin lifting up easily, and at the same time the moving platform continues to gradually slide forward until it reaches the point where balancing the control system can be activated. Once the wheelchair is traveling along on its back wheels and the moving platform has stopped sliding, the balancing process can begin. Figure 2 presents the four transition phases involved in changing the wheelchair$'s$ COG.

2.3 Dynamic Model of a two-wheeled wheelchair

In this section, we describe a mathematical model of the wheelchair when it remains upright on two wheels. The wheelchair is considered to be a single link inverted pendulum. The non-linear dynamic model is analyzed based on derivation via the Euler-Lagrange equation of motion, and under the assumption that there is no slippage between the wheels and the ground. The details of the parameters used in the equations are defined in Appendix.

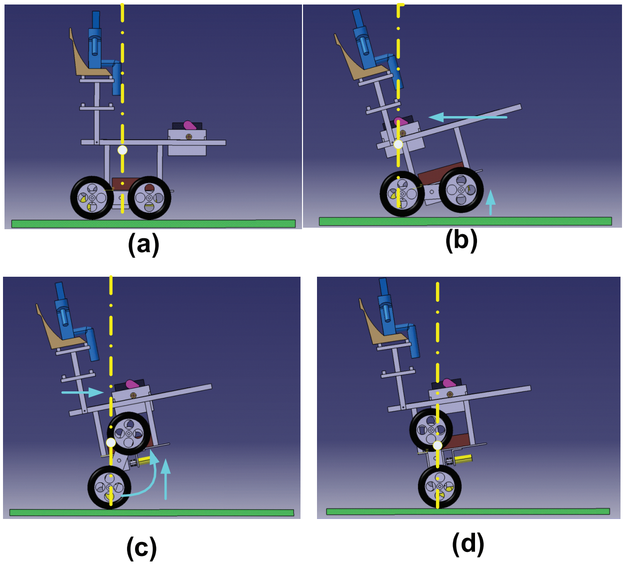

Fig. 2. The four transition phases for changing the COG: (a) four-wheel function; (b) COG is moving backward; (c) transition phase; and (d) balancing.

In order to obtain the wheelchair model, let us consider the system in two separate links, which are comprised of Link 1 and Link 2, as illustrated in Figure 3. Link 1 is composed of the rear wheels, whereas the front wheels and payload are considered as Link 2. One can write the kinetic energy of Link 1 as follows:

$$K_1 = \frac{1}{2} m_1 \dot{Z}_1^2 + \frac{1}{2} J_1 \frac{\dot{Z}_1^2}{l_1} \quad (1)$$

Similarly, the kinetic energy of Link 2 can be expressed as:

$$K_2 = \frac{1}{2} m_2 (\dot{Z}_1^2 + 2\dot{Z}_1 l_2 \dot{\theta}_2 \cos\theta_2 + l_2^2 \dot{\theta}_2^2) + \frac{1}{2} J_2 \dot{\theta}_2^2 \quad (2)$$

A summation of Eq. (1) and Eq. (2) produces the total kinetic energy in the system, K_T. Since the potential energy of Link 1 is zero, the total potential energy, P_T, is only derived from Link 2, or $P_T = m_2 g l_2 \cos\theta_2$. The Lagrangian function is therefore stated as follows:

$$\begin{aligned} L &= K_T - P_T \\ &= \frac{1}{2}(m_1 + m_2 + J_1)\dot{Z}_1^2 + \frac{1}{2}(m_2 l_2^2 + J_2)\dot{\theta}_2^2 \\ &\quad + m_2 \dot{Z}_1 \dot{\theta}_2 l_2 \cos\theta_2 - m_2 g l_2 \cos\theta_2 \end{aligned} \quad (3)$$

Assuming there is no viscous force occurring in the system, solving the Lagrange equations yields:

$$u = (m_1 + m_2 + J_1 \frac{1}{l_1^2})\ddot{Z}_1 + m_2 \ddot{\theta}_2 l_2 \cos\theta_2 - m_2 l_2 \dot{\theta}_2^2 \sin\theta_2 \quad (4)$$

and

$$0 = (m_2 l_2^2 + J_2)\ddot{\theta}_2 + m_2 \ddot{Z}_1 l_2 \cos\theta_2 - m_2 g l_2 \sin\theta_2 \quad (5)$$

This can be rewritten as:

$$\ddot{\theta} = \alpha - \beta \quad (6)$$

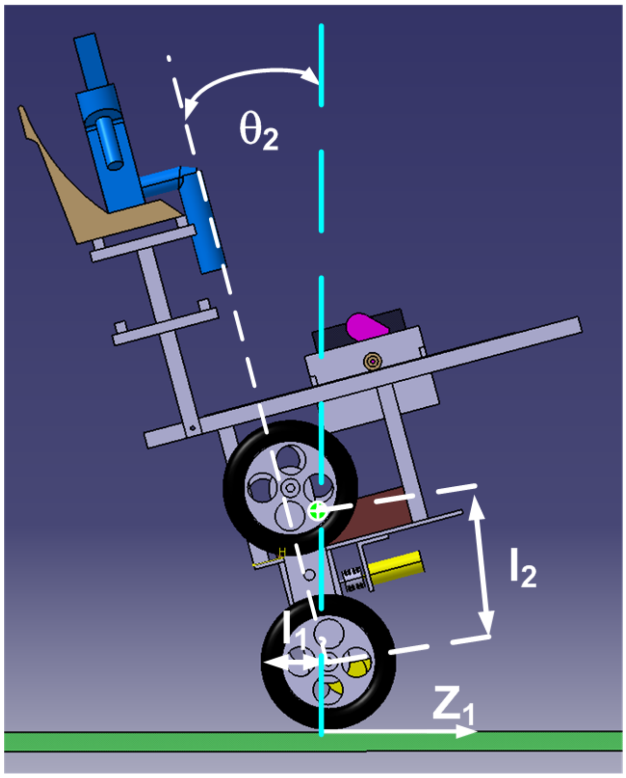

Fig. 3. Two-link wheelchair

where

$$\alpha = \frac{(m_2 l_2 g \sin\theta)(m_1 + m_2 + \frac{J_1}{l_1^2})}{((m_2 l_2^2 + J_2)(m_1 + m_2 + \frac{J_1}{l_1^2})) - (m_2 l_2 \cos\theta)^2}$$

$$\beta = \frac{(m_2 l_2 \cos\theta)u + (m_2^2 l_2^2 \cos\theta \sin\theta)\dot{\theta}^2}{((m_2 l_2^2 + J_2)(m_1 + m_2 + \frac{J_1}{l_1^2})) - (m_2 l_2 \cos\theta)^2}$$

and

$$\ddot{z} = \chi - \delta \quad (7)$$

where

$$\chi = \frac{(m_2 l_2^2 + J_2)u + ((m_2 l_2^2 + J_2)((m_2 l_2 \sin\theta)\dot{\theta}^2)}{((m_2 l_2^2 + J_2)(m_1 + m_2 + \frac{J_1}{l_1^2})) - (m_2 l_2 \cos\theta)^2}$$

$$\delta = \frac{(m_2^2 l_2^2 g \sin\theta \cos\theta)}{((m_2 l_2^2 + J_2)(m_1 + m_2 + \frac{J_1}{l_1^2})) - (m_2 l_2 \cos\theta)^2}$$

Since the objective is to keep the pendulum upright, it seems reasonable to assume that θ(t) and $\dot{\theta}$(t) will remain close to zero. The non-linear model is thus linearized, in order to simplify the analysis and design of the controllers, using these approximations: $\sin\theta \approx \theta$, $\cos\theta \approx 1$, $\theta x \theta \approx 0$, $\dot{\theta} x \dot{\theta} \approx 0$. Eq. (1), and Eq. (2) are reduced to:

$$\ddot{\theta} = \widetilde{\alpha} - \widetilde{\beta} \quad (8)$$

where

$$\widetilde{\alpha} = \frac{(m_1 + m_2 + \frac{J_1}{l_1^2})(m_2 l_2 g)\theta}{((m_2 l_2^2 + J_2)(m_1 + m_2 + \frac{J_1}{l_1^2})) - (m_2 l_2)^2}$$

$$\widetilde{\beta} = \frac{(m_2 l_2)u}{((m_2 l_2^2 + J_2)(m_1 + m_2 + \frac{J_1}{l_1^2})) - (m_2 l_2)^2}$$

$$\ddot{z} = \widetilde{\chi} - \widetilde{\delta} \tag{9}$$

where

$$\widetilde{\chi} = \frac{(m_2 l_2^2 + J_2)u}{((m_2 l_2^2 + J_2)(m_1 + m_2 + \frac{J_1}{l_1^2})) - (m_2 l_2)^2}$$

$$\widetilde{\delta} = \frac{(m_2^2 l_2^2 g)\theta}{((m_2 l_2^2 + J_2)(m_1 + m_2 + \frac{J_1}{l_1^2})) - (m_2 l_2)^2}$$

Choosing the states $x_1 = \theta$, $x_2 = \dot{\theta}$, $x_3 = z$ and $x_4 = \dot{z}$, we obtain the following state model

$$\dot{x} = Ax + bu \tag{10}$$

where

$$A = \begin{bmatrix} 0 & 1 & 0 & 0 \\ K_1 & 0 & 0 & 0 \\ 0 & 0 & 0 & 1 \\ K_3 & 0 & 0 & 0 \end{bmatrix}; b = \begin{bmatrix} 0 \\ K_2 \\ 0 \\ K_4 \end{bmatrix}$$

and the parameterts are:

$$K_1 = \frac{(m_1 + m_2 + \frac{J_1}{l_1^2})(m_2 l_2 g)}{((m_2 l_2^2 + J_2)(m_1 + m_2 + \frac{J_1}{l_1^2})) - (m_2 l_2)^2}$$

$$K_2 = \frac{-(m_2 l_2)}{((m_2 l_2^2 + J_2)(m_1 + m_2 + \frac{J_1}{l_1^2})) - (m_2 l_2)^2}$$

$$K_3 = \frac{-(m_2^2 l_2^2 g)}{((m_2 l_2^2 + J_2)(m_1 + m_2 + \frac{J_1}{l_1^2})) - (m_2 l_2)^2}$$

$$K_4 = \frac{(m_2 l_2^2) + J_2}{((m_2 l_2^2 + J_2)(m_1 + m_2 + \frac{J_1}{l_1^2})) - (m_2 l_2)^2}$$

3. FUZZY CONTROLLER FOR STABILIZING

This section discusses the design of the FLS, which is used to control the stability and mobility of the wheelchair. Figure 4 demonstrates the block diagram for controlling its pitch angle, and for stopping the motion while maintaining stability on two-wheels. It is evident that the FLS is

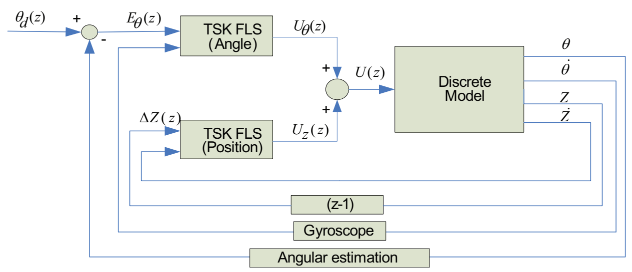

Fig. 4. Block diagram showing the pitch and wheel direction control based on the FLS scheme

designed to handle the discrete time model, which is obtained by discretizing Eq. (10), by using a sampling rate of 1 KHz. The inputs to the upper FLS are the angle error E_θ(z) and the angular velocity $\dot{\theta}$(z), Meanwhile, the force U_θ(z) is defined as the output. The objective of the upper FLS is to generate some force, so that the wheelchair can incline to its desired angle θ_d(z). which is, in this case, θ_d=0. For the lower FLS, the one-time step difference of the distance and the velocity is inputted to the FLS. The output U_Z(z) is generated to stop the motion after it has reached a steady state. The sum of U_θ(z) and U_Z(z) is then applied to the wheelchair (rear wheels).

The following subsections will provide brief overviews of type-1 TSK FLS, and interval type-2 TSK FLS, as used in the block diagram in Figure 4. Later on, the same type of FLS is deployed in the upper and lower blocks, in order to compare the effectiveness of the type-1 and type-2 designs.

3.1 Zero-Order Type-1 TSK FLS

Two zero-order type-1 TSK models are considered in this section, with a rule base of 25 rules, and with each having 2 antecedents. The rules are shown in Table 1. The first model, as highlighted, is designed to achieve the desired angle, which is zero degree in our work, while the second model is used for stopping the motion of the wheelchair after it has reached a steady state.

Table 1. Type-1 Fuzzy rules for controlling the angle and displacement

E_θ / ΔZ \ $\dot{\theta}$ / $\dot{Z}$	NB	NS	ZO	PS	PB
NB	PM / PBB	PB / PBB	PB / PB	PBB / PB	PBB / PM
NS	PS / PBB	PM / PB	PB / PB	PB / PM	PBB / PS
ZO	NM / PM	NS / PS	ZO / ZO	PS / NS	PM / NM
PS	NBB / NS	NB / NM	NB / NB	NM / NB	NS / NBB
PB	NBB / NM	NBB / NB	NB / NB	NB / NBB	NM / NBB

The antecedents shown in Figure 5 are type-1 fuzzy sets. Meanwhile, the consequents presented in Figure 6 are designed as crisp numbers to reduce computational complexity. The output of type-1 TSK FLS is obtained as:

$$y_{TSK}(x) = \frac{\sum_{i=1}^{M} f^i(x) y^i(x)}{\sum_{i=1}^{M} f^i(x)} \tag{11}$$

where $y^i(x)$ is the output of the i^{th} rule. and $f^i(x)$ is the rule firing level, which is defined as:

$$f^i(x) = min\left[\mu_{F_1^i}(x_1), \mu_{F_2^i}(x_2)\right] \tag{12}$$

The parameter $\mu_{F_k^l}(x_k)$ denotes the membership function of the antecedent k in rule l.

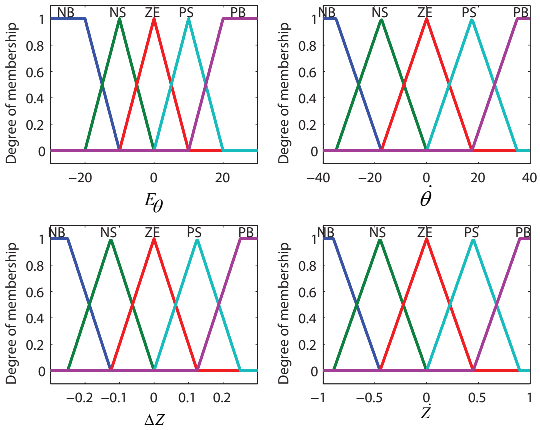

Fig. 5. Primary membership functions of the antecedents.

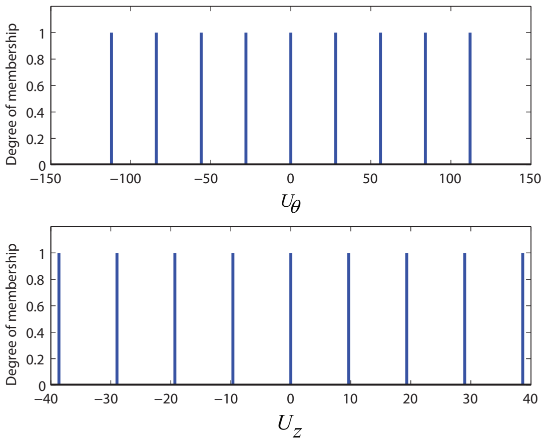

Fig. 6. The consequents.

3.2 Interval Type-2 TSK FLS

A zero-order interval type-2 TSK model is considered next, which has the same rules and number of antecedents as the type-1 model. The only difference is in respect to the primary memberships of the inputs containing the uniformly shaded FOUs in the fuzzy sets, as depicted in Figure 7. Kindly note the secondary membership functions are interval sets.

Let $\underline{\mu}_{\widetilde{F}_k^l}(x_k)$ and $\overline{\mu}_{\widetilde{F}_k^l}(x_k)$ denote the lower and upper membership functions for $\mu_{\widetilde{F}_k^l}(x_k)$ where $k = 1, 2$ (number of antecedents) and $l = 1, 2, 3, ..., 25$ (number of rules). For an interval type-2 TSK FLS, the results of the input and antecedent operations is an interval type-1 set, wherein the firing interval, is a set of $\left[\underline{f}^l, \overline{f}^l\right]$ that is determined by using a definition of the minimum t-norm as follows:

$$\underline{f}^i(x) = min\left[\underline{\mu}_{\widetilde{F}_1^l}(x_1), \underline{\mu}_{\widetilde{F}_2^l}(x_2)\right]$$
$$\overline{f}^i(x) = min\left[\overline{\mu}_{\widetilde{F}_1^l}(x_1), \overline{\mu}_{\widetilde{F}_2^l}(x_2)\right] \tag{13}$$

The fired output consequent $\mu_{\widetilde{B}^l}(y)$ of rule R^l can be obtained from the fuzzy rules demonstrated in Table 1.

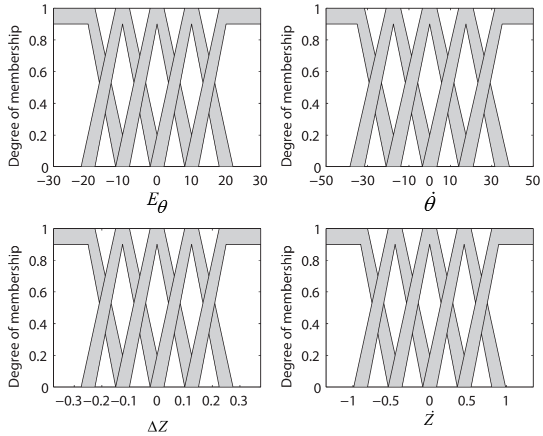

Fig. 7. Pictorial representation of a type-2 fuzzy set.

For a type reduction, and interval set determined by its two end points, this can be expressed as follows:

$$y_l = \frac{\sum_{i=1}^{M} \underline{f}^i y_l^i}{\sum_{i=1}^{M} \underline{f}^i}$$
$$y_r = \frac{\sum_{i=1}^{M} \overline{f}^i y_r^i}{\sum_{i=1}^{M} \overline{f}^i} \tag{14}$$

where M is 25 in this design. We finally defuzzify the interval set using the average of:

$$y(x) = \frac{y_l + y_r}{2} \tag{15}$$

4. ANGULAR POSITION ESTIMATION BY KALMAN FILTERING

To maintain an upright position, the actual pitch angle of Link 2 must be compared with the desired angle in real time. The angular position of Link 2 is measured using an accelerometer and a gyroscope, which is attached to the wheelchair. Fusing data from both sensors is computed in real-time, based on the Kalman filter (KF). This yields relatively accurate and drift-free measurements.

An overview of the discrete time KF-based angular position estimation is derived in a simple manner (Panomruttanarug and Higuchi, 2010). The angle and rate read from the gyroscope are modeled in 1−D state space form as follows:

$$x(k+1) = Ax(k) + Bu(k) + w(k)$$
$$y^*(k) = Cx(k) \tag{16}$$

where $x(k)$ is a state vector of $\theta(k)$. $u(k)$ is the rate at the time step k, read from the gyroscope. $y^*(k)$ is the output angle from the Kalman filtering, and $w(k)$ denotes a plant noise with covariance of Q. $A = 1$, $B = \delta t$, and $C = 1$ are the Markov parameters of the system, where δt is the sampling time with a value of 10 ms.

One can write the Kalman filter equations with time varying gain, as follows:

$$\hat{x}(k+1|k) = A\hat{x}(k|k-1) + Bu(k) + AK(k)\left[\bar{y}(k) - C\hat{x}(k|k-1)\right] \quad (17)$$

$$K(k+1) = P(k+1)C^T(CP(k+1)C^T + R)^{-1}$$

$$P(k+1) = AP(k)A^T$$

$$-AP(k)C^T(CP(k)C^T + R)^{-1}CP(k)A^T + BQB^T$$

where P is the error covariance of the one step ahead state prediction, which is used to compute the Kalman gain K. One obtains the true filter estimates from:

$$\hat{x}(k+1|k+1) = \left[I - K(k+1)C\right]\left[A\hat{x}(k|k) + Bu(k)\right] + K(k+1)\bar{y}(k+1) \quad (18)$$

Data from the accelerometer is used as the measurement $\bar{y}$ in (18), which has a covariance of R. Kindly note that some comments relating to picking the values of covariance Q and R, will be discussed in the experimental results section.

5. SIMULATION, EXPERIMENTAL RESULTS AND DISCUSSION

5.1 Mechatronic Design

In this section, details of the hardware design will be provided. Figure 8 displays the photographs of the balancing wheelchair. The wheelchair is composed of four 24V DC motors, which are connected to each wheel, and a 12V DC motor that is mounted to the moving platform. Each motor is equipped with an encoder and a H-bridge motor drive module. Two 12V lead-acid batteries are connected in series to supply power to the motor drive modules, along with two microcontrollers dsPIC30F4011 from Microchip. One of the microcontrollers is used to execute the control algorithm (self-balancing control), while the other is responsible for generating appropriate pulses to the motors and reading back signals from the sensors.

In order to estimate the pitch angle, data from a gyroscope, LPR510AL, and an accelerometer, MMA7361L, are combined using the filtering method as described in the previous section. Figure 9 shows the system structure of the wheelchair system.

Fig. 8. Prototype of balancing wheelchair

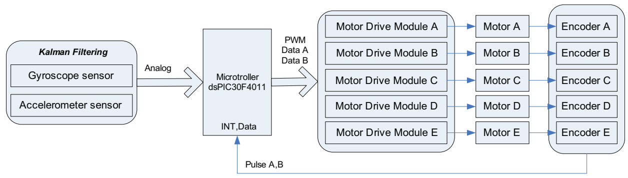

Fig. 9. Control architecture of the overall system

Table 2. Physical parameters for simulation results

Parameter	Value
m_1	3.2 kg
m_2	36.176 kg
l_1	0.145 m
l_2	0.4025 m
J_1	0.025024
J_2	1.73634
g	9.81 m/s^2

5.2 Simulation Results

This section presents the simulation results using the parameters of the dynamic model, as provided in Table 2.

Based on the assumption that the initial angle is at -5 deg, the performance of the two proposed controllers is compared and shown in Figure 10. The plot in the upper left corner shows how well they can track the desired zero angle. It is evident that both of them can track the desired angle within a few seconds. However, type-1 seems to have 35% lower %OS with a 1.3 times longer settling time. Based on the current information, it is unclear which one performs better. The plot in the lower left corner gives us more information about the displacement of the wheelchair. Type-2 stops moving around 0.38m from the original position, while type-1, stays steady at 0.43m from the original position. As a result, type-2 performs better in the sense that it can reach a steady state and stop moving faster. The angular and linear velocity of the wheelchair are demonstrated in the upper right and lower right corners, respectively.

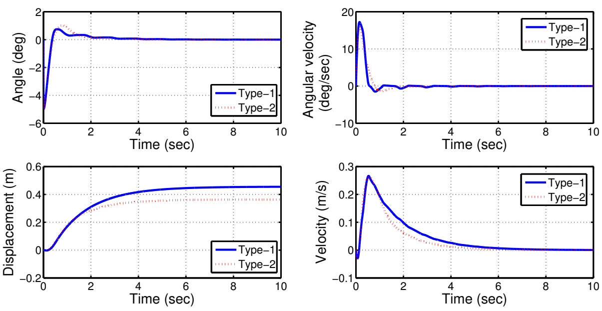

Fig. 10. Comparison of type-1 and type-2 TSK FLS with the initial angle at -5 deg

Figure 11 illustrates the tracking error of the angle (upper), and the total force applied to the wheelchair, in order to obtain the desired response (lower). As seen in Figure 10, type-1 and type-2 perform slightly different in respect to tracking the angle according to the angle error plot.

However, type-2 requires more significant force to push the angle back to zero and to reach steady state. Kindly note also that the maximum required force for type-1 is about -40N, as compared to -70N for type-2. Therefore, consideration must be given to determine whether it is reasonable to use type-2, which requires more force, but less settling time, in respect to real world applications.

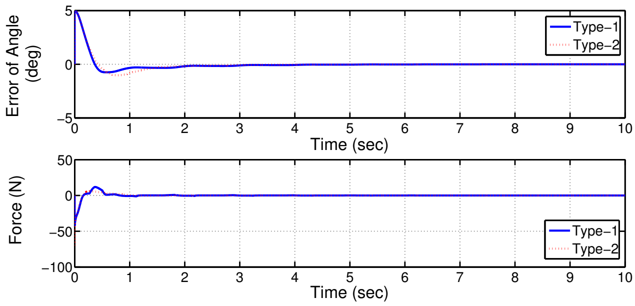

Fig. 11. Angle error (upper) and force applied to the wheelchair (lower) corresponding to Figure 10

Since the steady state responses of the angle using type-1 and type-2 are exactly the same, let us consider the comparison of transient responses using both controllers. For different initial angles, Table 3 summarizes the characteristics of the transient responses, wherein comparisons are made between the two controller designs. The performance of type-1 is shown in the shaded area.

It is evident that type-2 gives a slightly slower rise time and a larger %OS, and also provides a noticeably better performance in regard to settling time and displacement in all cases. However, more force is required to achieve the desired response in a faster time.

Table 3. Performance indicators in transient responses of the angle at different initial angles

Initial angle (deg) \ Response	Rise time (sec) Type-1	Rise time (sec) Type-2	Settling time (sec) Type-1	Settling time (sec) Type-2	%OS Type-1	%OS Type-2	Displacement (m) Type-1	Displacement (m) Type-2
-5	0.370	0.430	5.3	4.6	15.00	20.40	0.45	0.36
-10	0.396	0.408	6.4	5.2	15.20	18.70	0.96	0.70
-15	0.358	0.351	6.4	5.4	21.00	24.60	1.27	0.89
-20	0.353	0.348	6.66	5.2	36.40	38.7	1.21	0.94
-25	0.364	0.364	5.9	4.9	46.4	49.20	1.23	0.99
-30	0.382	0.384	1.71	1.72	55.93	57.33	0.96	1.05

5.3 Experimental Results

This section is devoted to the extensive experiments conducted to verify the wheelchair performance using the proposed fuzzy logic schemes.

Before starting the stabilizing process, the wheelchair is initially set to its four-wheel mode, as seen in Figure 12 (a). The movable platform is subsequently slid backward, thus producing sufficient torque to lift the front wheels, as displayed in Figure 12 (b). In Figure 12 (c), the front wheels (casters) start lifting, and the moving platform quickly slides forward to help balance the wheelchair. Figure 12 (d) illustrates the final upright position of the wheelchair.

The balancing control system, which is based on the fuzzy control approach, is therefore operating in real time to maintain stability.

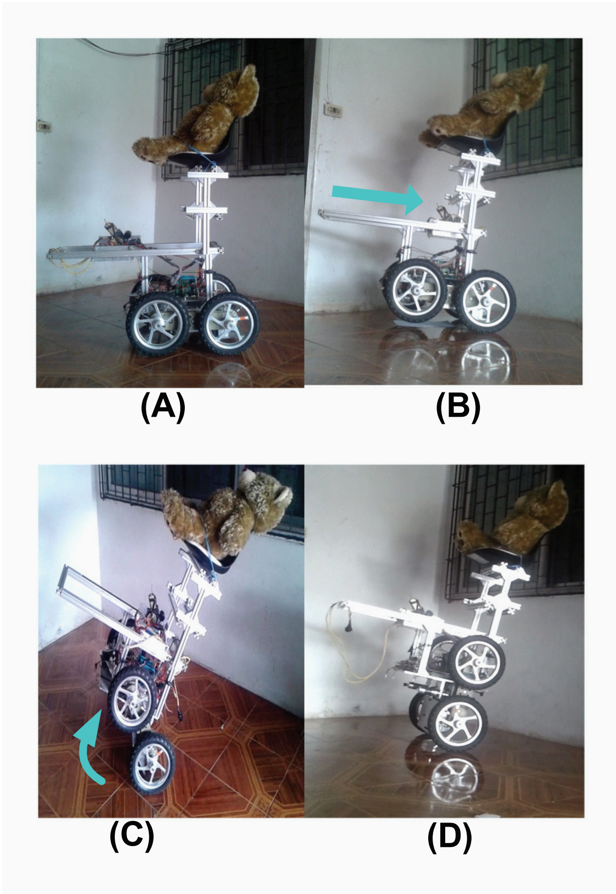

Fig. 12. Lifting procedure

In order to obtain an angular position, the statistical properties of the gyroscope (plant), accelerometer (measurement), and approximate noise covariance matrices were observed as: $Q = 1.859\times10^{-5}$ and $R = 6.989\times10^{-5}$. Figure 13 demonstrates a comparison between the tracking angle, which was read from the sensors and calculated from Kalman filtering, when it was pitched up and down. It is clearly evident that the tracking angle from the fusing algorithm closely follows the gyroscope readings, since the noise covariance matrices suggest that the accelerometer is less reliable, i.e., $R>Q$. As a result, it is not recommended that a single value is used for Q and R.

The next example is demonstrated when Q and R are varied in accordance with the angular velocity. Table 4 gives the noise covariance matrices that correspond to each range of angular velocity. The values are adjusted based on a heuristic approach, with the assumption that the

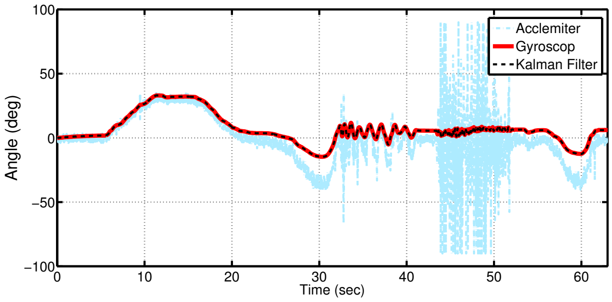

Fig. 13. Tracking angular using $Q = 1.859{\times}10^{-5}$ and $R = 6.989{\times}10^{-5}$

Table 4. Adjustable noise covariance matrices

	Angular velocity (deg/sec)				
	±6	±15	±30	±60	Other
Q	0.0399	0.0099	0.0099	0.0099	0.0099
R	0.4989	0.7122	2.1222	3.1223	4.9370

gyroscope is more reliable when it is pitched at a high angular rate.

Figure 14 illustrates the results that are associated with the noise covariance matrices that are provided in Table 4. The tracking results from the Kalman filter provides a good estimation, even when there are sudden vibrations lasting around 40 to 60 seconds.

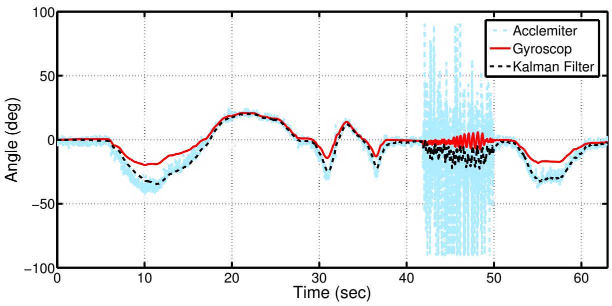

Fig. 14. Tracking angular using noise covariance matrices in Table 4

Subsequently, an implementation of the controller designs, together with the adjustable noise covariance matrices, is carried out. For comparative study, we will investigate performance of the wheelchair using the controller designs on different floor types composed of a carpet floor, a cement floor, and a tile flooring. The first experiment is performed on a carpet floor having a highest roughness value among the 3 surfaces. Starting from the initial angle, which is around zero degrees, the performance of the two proposed controllers are compared and shown in Figure 15.

The upper sub-plot shows how well they stabilize in the upright position, by staying at zero degrees, while the lower sub-plot gives information on how far the wheelchair moves from its original position. Using type-1, the wheelchair swings slowly back and forth, and makes some moves to maintain stability. When it reaches 30 seconds, it starts to shake a lot, and loses control by falling off at around 50

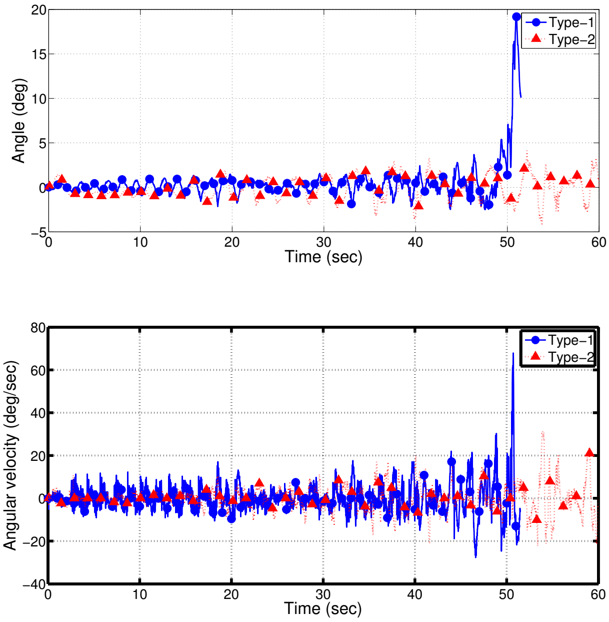

Fig. 15. Comparison of Type-1 and Type-2 FLS on a carpet floor: (a) Angle (b) Angular velocity

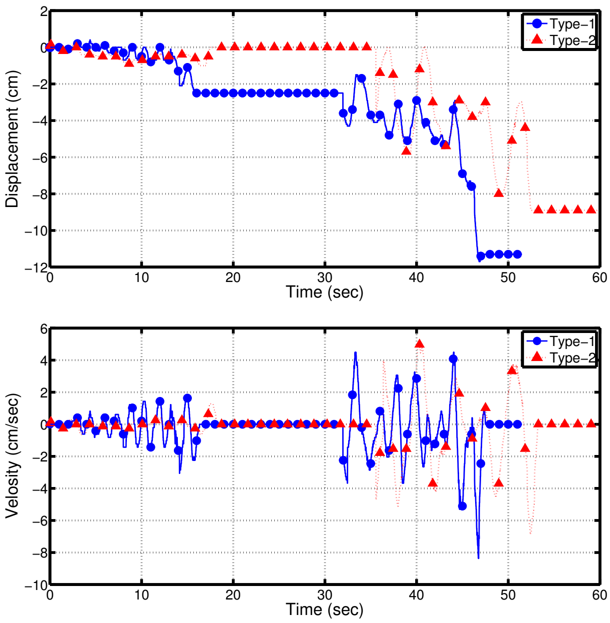

Fig. 16. Comparison of Type-1 and Type-2 FLS on a carpet floor: (a) Displacement (b) Linear velocity

sec. On the other hand, the wheelchair with type-2 stands nearly still for about 35 seconds, before it gradually swings and causes some back and forth motion and eventually falling off at approximately 60 seconds. As a result, type-2 FLC performs better in the sense that it retains the wheelchair in an upright position for a longer period of time and with less swinging motion.

Figure 16 provides the corresponding angular velocity (top) and linear velocity (bottom) from the experiment. The associated force is illustrated in Figure 17. Numerous experiments have been extensively performed to verify the effectiveness of the controller designs. Type-1 and type-2 are able to hold themselves in an upright position for 54 seconds and 70 seconds on average.

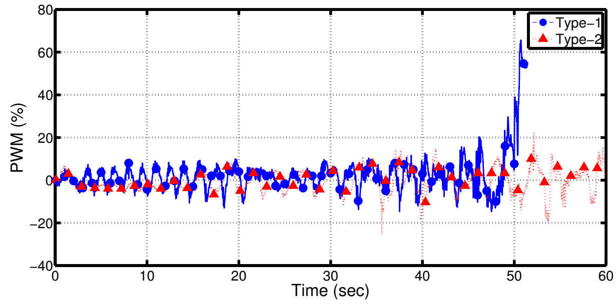

Fig. 17. Force applied to the wheelchair corresponding to Figure 15 and Figure 16

The next experiment is performed on a cement floor. Figures 18, 19, and 20 show a similar plot as in Figures 15, 16, and 17. Since the roughness value of a cement floor is slightly lower than that of a carpet floor, the time that two controllers can maintain stability does not change much in this case. By performing numerous experiments, average times to maintain an upright position for type-1 and type-2 are 41 seconds and 52 seconds, respectively. Again, it is evident that type-2 performs better than type-1.

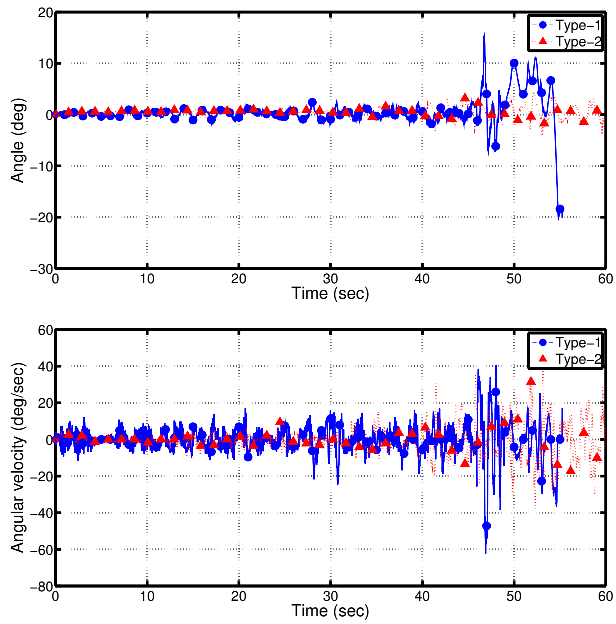

Fig. 18. Comparison of Type-1 and Type-2 FLS on a cement floor: (a) Angle (b) Angular velocity

The last experiment is performed on a tile flooring having the lowest roughness value. Figures 21, 22, and 23 give a new set of plots similar to Figures 18, 19, and 20. By comparing Figures 18 and 21, it is clear that the controllers show a poorer performance on a slippery surface. The average time to maintain an upright position for type-1 and type-2 has been reduced to 22 seconds and 33 seconds, respectively. However, type-2 still performs better than type-1.

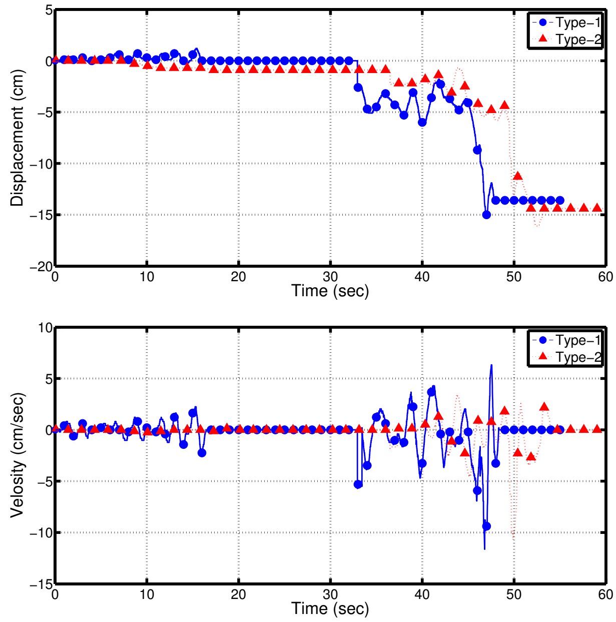

Fig. 19. Comparison of Type-1 and Type-2 FLS on a cement floor: (a) Displacement (b) Linear velocity

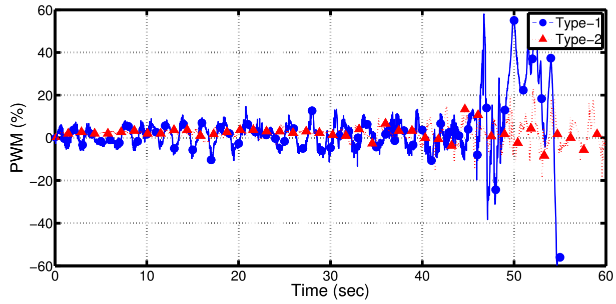

Fig. 20. Force applied to the wheelchair corresponding to Figure 18 and Figure 19

6. CONCLUSIONS

In this paper, we have designed and constructed a stand-up wheelchair that is able to lift up its front wheels to adjust the vertical height with affordable electronic components. The mechanical structure for changing the posture of the wheelchair is designed to move the wheelchair's COG. Once the wheelchair is set to its initial point, the balancing process can begin. To achieve a stable upright position, we have applied control systems using type-1 FLC and type-2 FLC. Both fuzzy logic controllers have been designed with the objective of obtaining a zero angle response with zero displacement. The fuzzy rules are designed to be simple and straightforward so they can be implemented in experiments without the use of complicated computations. However, a Kalman filter is required to handle uncertainties from noisy sensors. We have developed a strategy to adjust noise covariance matrices, used in Kalman filtering, corresponding to the angular velocity. By comparison, through simulations and experimental results, it was discovered that the type-2 FLS performs more effectively, and provides better results with respect to stabilizing the wheelchair in an upright position. Extended experiments have been carried out to investigate the effectiveness of

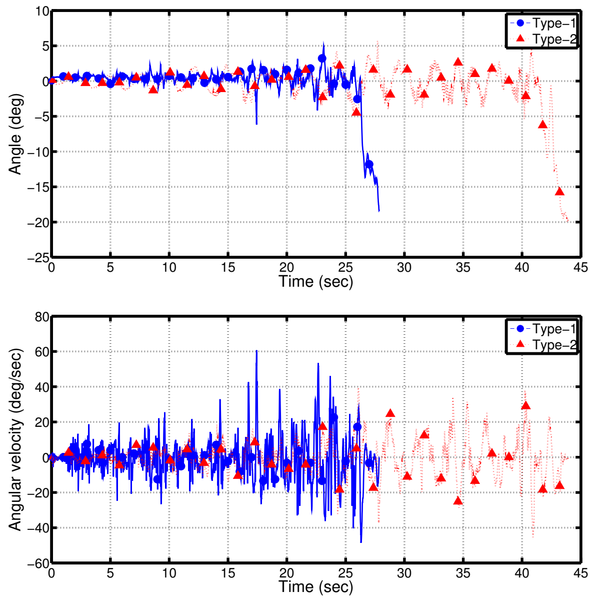

Fig. 21. Comparison of Type-1 and Type-2 FLS on a tile flooring: (a) Angle (b) Angular velocity

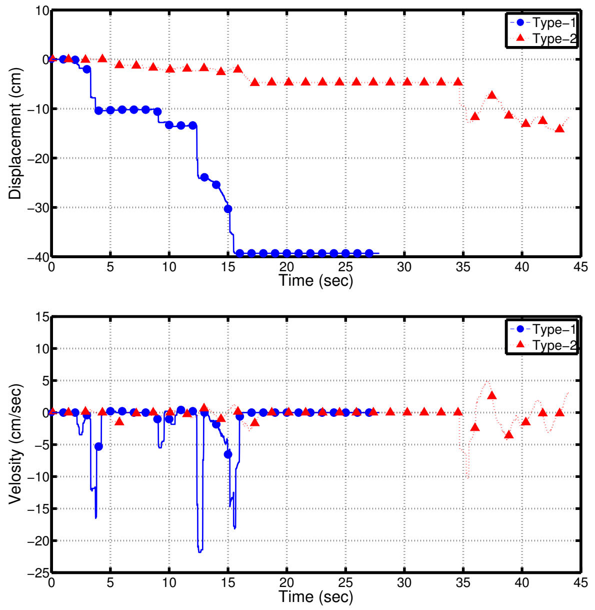

Fig. 22. Comparison of Type-1 and Type-2 FLS on a tile flooring: (a) Displacement (b) Linear velocity

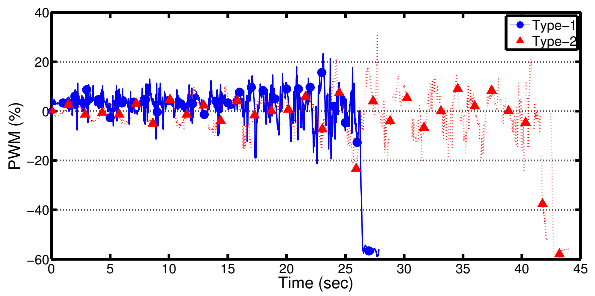

Fig. 23. Force applied to the wheelchair corresponding to Figure 21 and Figure 22

the balancing controllers when performing on different levels of roughness. It has been seen that the wheelchair can balance itself on the carpet floor for longer than on the cement floor, and longer than on the tile flooring, respectively.

ACKNOWLEDGEMENTS

This work was supported by National Research Council of Thailand (NRCT).

REFERENCES

Adhikary, N., and Mahanta, C. (2013). Integral backstepping sliding mode control for underactuated systems: Swing-up and stabilization of the Cart-Pendulum System, *ISA Transactions*, Vol.52, Issue6, pp.870-880.

Ahmad, S., Siddique, N. H., and Tokhi, M. O. (2011). A Modular Fuzzy Control Approach for Two-Wheeled Wheelchair, *Journal of Intelligent & Robotic Systems*, Vol.64, Issue3-4, pp.401-426.

Ahmad, S., Siddique, N. H., and Tokhi, M.O. (2014). Modelling and simulation of double-link scenario in a two-wheeled wheelchair, *Integrated Computer-Aided Engineeringl*, Vol. 21, No.2, pp.119-132.

Aracil, J., Acosta, J.*á*. and Gordillo, F. (2013). A nonlinear hybrid controller for swinging-up and stabilizing the Furuta pendulum, *Control Engineering Practice*, Vol.21, Issue8, pp.989-993.

Bardini, M. E. and El-Nagar, A. M. E. (2014). Interval type-2 fuzzy PID controller for uncertain nonlinear inverted pendulum system, *ISA Transactions 53*, pp.732-743.

Bettayeb, M., Boussalem, C., Mansouri, R. and Saggaf, U.M. A. (2001). Almost global stabilization of the inverted pendulum via continuous state feedback, *Automatica*, Vol.37, Issue7, pp.1103-1108.

Bettayeb, M., Boussalem, C., Mansouri, R. and Al-Saggaf, U.M. (2014). Stabilization of an inverted pendulum-cart system by fractional PI-state feedback, *ISA Transactions*, Vol.53, Issue2, pp.508-516.

Chan, R. P. M., Stol, K. A. and Halkyard, C. R. (2013). Review of modelling and control of two-wheeled robots, *Annual Reviews in Control*, Vol.37, Issue1, pp. 89-103.

Durand, S., Guerrero-Castellanos, J. F., Marchand, N. and Guerrero-Sánchez, W. F. (2013). Event-Based Control of the Inverted Pendulum: Swing up and Stabilization, *Journal of Control Engineering and Applied Informatics*,Vol.15, No. 3, pp. 96-104.

Graichen, K., Treuer, M. and Zeitz, M. (2007). Swing-up of the double pendulum on a cart by feedforward and feedback control with experimental validation, *Automatica*, Vol.43, Issue1, pp.63-71.

iBOT http://www.dekaresearch.com/ibot.shtml. *Nonlinear Dynamics*, Vol.70, Issue1, pp.767-777.

Ibáñez, C. A., Suarez-Castanon, M. S. and Cruz-Cortés, N. (2012). Output feedback stabilization of the inverted pendulum system: a Lyapunov approach,

Mon, Y.J. and Lin, C.M. (2014). Double inverted pendulum decoupling control by adaptive terminal sliding-mode recurrent fuzzy neural network, *Journal of Intelligent and Fuzzy Systems*, Vol.26, pp.1723-1729.

Noh, J. S., Lee, G. H., and Jung, S. (2010). Position Control of a Mobile Inverted Pendulum System Using

Radial Basis Function Network, *International Journal of Control, Automation and Systems*, Vol.8, Issue1, pp.157-162.

Olson, Z.L., Moorhem, W.K. V. and Roemer, R.B. (2006). A comparative analysis of three self-balancing wheelchair balancing mechanisms, *IEEE Trans Neural Syst Rehabil Eng*, pp.481-491.

Panomruttanarug, B. and Higuchi, K. (2010). Fuzzy Logic Based Autonomous Parallel Parking System with Kalman Filtering, *SICE Journal of Control, Measurement, and System Integration*, pp.266-271.

Panomruttanarug, B. and Chotikunnan, P. (2014). Self-Balancing iBOT-Like Wheelchair Based on Type-1 and Interval Type-2 Fuzzy Control, *11th International Conference on Electrical Engineering Electronics, Computer, Telecommunications and Information Technology (ECTI-CON).*

Rubi, J., Rubio, A. and Avello, A. (2002). Adaptive Fuzzy Switched Swing-Up and Sliding Control for the Double-Pendulum-and-Cart System, *Control Theory and Applications, IEE Proceedings*, Vol.149, Issue2, pp.169-175.

Segway http://www.segway.com.

Tao, C. W., Taur, J., J.H., C. and Su, S.F. (2010). Adaptive Fuzzy Switched Swing-Up and Sliding Control for the Double-Pendulum-and-Cart System, *IEEE Transactions*, Vol.40, Issue1, pp.241-252.

Yi, J., Yubazaki, N. and Hirota, K. (2001a). Systematic design method of stabilization fuzzy controllers for pendulum systems, *International Journal of Intelligent Systems*, Vol.16, Issue8, pp.983-1008.

Yi, J., Yubazaki, N. and Hirota, K. (2001b). Stabilization control of series-type double inverted pendulum systems using the SIRMs dynamically connected fuzzy inference model, *Artificial Intelligence in Engineering*, Vol.15, Issue3, pp.297-308.

Yi, J., Yubazaki, N. and Hirota, K. (2002). A new fuzzy controller for stabilization of parallel-type double inverted pendulum system, *Fuzzy Sets and Systems*, Vol.126, Issue1, pp.105119.

Appendix A.

L	The total Lagrangain
K_T	The total kinetic energy in the system
P_T	The total potential energy
g	Gravitational force
u	Input of the system
Z	Linear displacement of robot
$\dot{Z}$	Linear velocity of robot
$\ddot{z}$	Linear acceleration of robot
θ	Rotation angle of robot
$\dot{\theta}$	Angular velocity of robot
$\ddot{\theta}$	Angular acceleration of robot
Z_1	Linear displacement of wheel (Link1)
$\dot{Z}_1$	Linear velocity of wheel (Link1)
θ_2	Rotation angle of Link2
$\dot{\theta}_2$	Angular velocity of Link2
m_1	Mass of wheel (Link1)
m_2	Mass of Link2
J_1	Moment of inertia of wheel (Link1)
J_2	Moment of inertia of Link2
l_1	Radius of wheel (Link1)
l_2	The radius is the length of the rod (Link2)